

# Two-Dimensional Hydrodynamics of Pre-Core Collapse: Oxygen Shell Burning

Grant Bazán<sup>1</sup>

David Arnett<sup>2</sup>

Steward Observatory, University of Arizona, Tucson, AZ 85721

## ABSTRACT

By direct hydrodynamic simulation, using the Piecewise Parabolic Method (PPM) code PROMETHEUS, we study the properties of a convective oxygen burning shell in a SN 1987A progenitor star ( $20 M_{\odot}$ ) prior to collapse. The convection is too heterogeneous and dynamic to be well approximated by one-dimensional diffusion-like algorithms which have previously been used for this epoch. Qualitatively new phenomena are seen.

The simulations are two-dimensional, with good resolution in radius and angle, and used a large (90-degree) slice centered at the equator. The microphysics and the initial model were carefully treated. Many of the qualitative features of previous multi-dimensional simulations of convection are seen, including large kinetic and acoustic energy fluxes, which are not accounted for by mixing length theory. Small but significant amounts of  $^{12}\text{C}$  are mixed non-uniformly into the oxygen burning convection zone, resulting in hot spots of nuclear energy production which are more than an order of magnitude more energetic than the oxygen flame itself. Density perturbations (up to 8 %) occur at the “edges” of the convective zone and are the result of gravity waves generated by interaction of penetrating flows into the stable region. Perturbations of temperature and  $Y_e$  (or neutron excess  $\eta$ ) at the base of the convective zone are of sufficient magnitude to create angular inhomogeneities in explosive nucleosynthesis products, and need to be included in quantitative estimates of yields. Combined with the plume-like velocity structure arising from convection, the perturbations will contribute to the mixing of  $^{56}\text{Ni}$  throughout supernovae envelopes. Runs of different resolution, and angular extent, were performed to test the robustness of these simulations.

*Subject headings:* convection - hydrodynamics - nucleosynthesis - stars: abundances - stars: evolution - supernovae: general

---

<sup>1</sup>e-mail: bazan@dirac.as.arizona.edu

<sup>2</sup>e-mail: darnett@as.arizona.edu

## 1. INTRODUCTION

Oxygen burning in a convective shell is one of the last, dominant burning stages before core collapse of a massive star. Its importance lies not just in the nucleosynthesis occurring by the nuclear burning itself, but also in the structure left by convection which might affect subsequent supernova evolution (Arnett 1969, Falk & Arnett 1973, Arnett et al. 1989). For instance, the division between the proto-neutron star and supernova ejecta, known as the “mass cut,” is expected to appear somewhere near the “edge” of the convective zone. Convection generated perturbations in density, velocity, entropy, and  $Y_e$  (or neutron excess  $\eta$ ) could alter the nature of core collapse as compared to spherically symmetric, one-dimensional calculations (Arnett 1977a, Burrows & Lattimer 1985, Bruenn 1985, Miller, et al., 1991; see Arnett 1996 for extensive discussion and references).

The bottom of the oxygen convective shell is expected to be the region where explosive nucleosynthesis occurs. Most iron peak isotopes are thought to be produced here. The most important individual product of this region would be  $^{56}\text{Ni}$ , which is responsible for powering supernova light curves and (after decay to Co) is the source of the 847 and 1208 keV  $\gamma$ -ray lines seen in SN1987A (Leising & Share 1990, Tueller et al. 1990, Kurfess et al. 1992, Palmer et al. 1993, Ait-Quamar et al. 1992). The explosive O- and Si-burning which produces  $^{56}\text{Ni}$  also produces other  $\gamma$ -ray emitting radionuclides such as  $^{44}\text{Ti}$  and  $^{57}\text{Ni}$  ( $^{57}\text{Co}$ ). Perturbations in  $Y_e$ , density, and temperature, left by convective O-burning, will *greatly* affect the relative abundances of individual isotopes, due to the sensitivity of nuclear statistical equilibrium (NSE) and quasiequilibrium to these parameters (Truran et al. 1966, Woosley et al. 1973, Arnett 1996). Studies of NSE have shown a neutron excess  $\eta = 1 - 2Y_e \approx 0.002$  best recreates the relative abundances of iron-peak nuclei, with slight changes in  $\eta$  altering relative abundances by large factors. A change in  $Y_e$  from 0.499 to 0.4995 changes the relative abundance of  $^{57}\text{Fe}$  to  $^{56}\text{Fe}$  by roughly a factor of 2.

We know from observations of SN 1987A that significant mixing of newly synthesized material throughout the envelope must occur (Arnett 1988, Pinto & Woosley 1988, Kumagai et al. 1989, Graham 1988). The only physical explanation that agrees with our understanding of massive star evolution is that significant density perturbations must appear at the interfaces of composition discontinuities and these result in Rayleigh-Taylor (and Richtmeyer-Meshkov) mixing in the ejecta (Falk & Arnett 1973, Benz & Thielemann 1990). This hypothesis has been tested with various fluid hydrodynamics codes by adopting ad hoc distributions of initial perturbation amplitude and length scale (Arnett et al. 1989, Fryxell et al. 1991, Müller et al. 1991, Arnett 1991, Hachisu et al. 1992, Herant & Benz 1992, Herant & Woosley 1994). On the whole, calculated  $^{56}\text{Ni}$  velocities were in agreement with observations for the bulk of the matter, but not for the highest speeds. Not enough Ni could be mixed to velocities as high as  $3,000 \text{ km s}^{-1}$ , which the observations imply. We believe that convective shell O-burning has a major effect on all of these phenomena.

In almost all hydrostatic stellar models, convection is treated by enforcing an adiabatic gradient, or better, some version of mixing length theory (Prandtl 1925, Vitense 1953, Böhm-

Vitense 1958; hereafter MLT). The basic tenets of MLT are that (1) convection occurring deep in stellar interiors results in an almost completely adiabatic structure, and that (2) excess energy flux (above that of radiative diffusion at the adiabatic gradient) is a function of the local superadiabatic gradient. The mixing of chemical species is approximated either by complete homogenization, or the use of a radial diffusion equation (when MLT formalism is applied). The concept of penetrative convection (overshoot from convective regions into adjacent radiative zones) is not a natural outcome of MLT, due to the local nature of the theory (Renzini 1987). Various ad hoc approaches to overshoot have been applied to stellar evolution; in most the overshoot distance is scaled to some multiple of the local pressure scale height.

Multi-dimensions simulations of turbulent compressible convection have revealed both the successes and shortcomings of MLT. One dynamical feature of convection, which has been present in every multi-dimensional simulation, is the asymmetry between up and down motions. Upward moving elements are typically broader in extent and slower than downward moving elements, although the degree of asymmetry is very dependent on the density contrast of the unstable region (Graham 1975, Hurlburt et al. 1984, Chan et al. 1982, Hurlburt et al. 1986, Chan & Sofia 1986, Cattaneo et al. 1991). As density contrast increases, so does the asymmetry (Hurlburt et al. 1984). Pressure fluctuations (the compressible nature of the fluid) can assist in driving descending motions, lead to buoyancy braking in ascending motions, and satisfy a Bernoulli relation with horizontal velocities (Hurlburt et al. 1986). The basic notion of buoyancy driven motions throughout most of the convective zone has been upheld, but at the boundaries, dissipation and compressibility are the dominant factors in the flow. In the more complex case, in which convective regions have nuclear timescales comparable to the mixing timescale, a kinetic (rather than steady state) description becomes crucial.

There are hints that the basic tenet in MLT regarding *energy* flux still holds true in multidimensional simulations. In both 2- and 3-D “large eddy” simulations, in which a sub-grid scale turbulence formalism (SGS) has been applied, vertical motions have been seen to breakup in less than the simulation dimension (Chan et al. 1982, Chan & Sofia 1986, Chan & Sofia 1989, Hossain & Mullan 1991). In fact, the autocorrelation of vertical velocity along vertical direction is a function of the difference in logarithmic pressure, but symmetric with a similar full width-half maximum (FWHM) across the entire computational regime (Chan et al. 1982, Chan & Sofia 1986). This means that the convective flux should be a function of the local pressure scale height. Amazingly, vertical velocities seem to be correlated over about one pressure scale height (Hossain & Mullan 1991), which is the range used for the past 30 years in stellar evolution models. However, even these positive indications are faulty. There seems to be a numerical dependence to these results: the correlation is no longer constant over an entire grid when the aspect ratio is increased (Chan & Sofia 1986) and the correlation length is dependent on the magnitude of the SGS turbulence included in the model. Indeed, in models where SGS turbulent viscosity has been omitted in favor of ordinary dynamical viscosity, no breakup of vertical motions has been observed (Hurlburt et al. 1984, Hurlburt et al. 1986).

Penetrative convection has also been modelled in multi-dimensions. In what follows, we will use a nomenclature in which *penetration* refers to mixing (in formally stable zones) that is efficient enough to weaken thermal stratification. Otherwise, edge mixing is referred to as *overshooting* (Massaguer et al. 1984). Fast downward plumes are responsible for extensive mixing of composition and energy from the unstable region into the lower stable region through gravity waves (Hurlburt et al. 1986), although a rapid increase in the stability of adjacent regions reduces the ability of plumes to penetrate (Hurlburt et al. 1994). Composition is advected across the stability boundary to a “penetration depth,” on the timescale for plume transit. In the case of true penetration, the region adjacent to the convective zone can be described by two layers: (1) where Peclet number  $> 1$ , adiabatic structure exists, and motions decelerate due to buoyancy breaking and (2) where Peclet number  $< 1$ , temperature perturbations damp out from radiative damping (Zahn 1991, Hurlburt et al. 1994). Note that the Peclet number is the ratio of the velocity scale  $v$  times the length scale  $\ell$ , to the thermal conductivity  $K$ ,  $Pec = v\ell/K$ , and a large Peclet number implies ineffective thermal energy transport relative to mass transport; see Landau & Lifshitz 1959. Our case, in which cooling is by  $\nu\bar{\nu}$  emission instead of radiative diffusion, does not seem to have been considered by the hydrodynamic community.

Shell oxygen burning differs from the canonical problem addressed by most previous multidimensional convection simulations. The convective regions of ZAMS A and F stars (Latour et al., 1981, Sofia & Chan 1984) and generic convection with ionization (Rast et al. 1993, Rast & Toomre 1993a, Rast & Toomre 1993b) are most comparable. However, such convective regions do not contain nuclear energy sources and neutrino energy sinks within the flow. It seems that local thermal effects, such as heating from ionization, can significantly affect convective flows. The treatment of convection affects neutrino cooled regions, since the efficiency of convection determines which adiabat a convective region can achieve. This in turn feeds back upon the neutrino emission (Aufderheide 1993, Arnett 1996).

In previous work (Arnett 1994, Bazán & Arnett 1994), we used our Piecewise Parabolic Method fluid dynamics code PROMETHEUS (Arnett et al. 1989) to begin an examination of the problem of the evolution of a O-burning shell in a  $20 M_{\odot}$ ,  $Z = 0.007$  star, prior to core collapse. Significant density perturbations (of the order of 7%) were found to occur at the boundaries of the convective region, along with non-uniform mixing of chemical species within the shell. Here, we present more extensive results of models of the same star, with different boundary conditions, grid sizes, and grid resolutions, and for a longer evolutionary time. We compare results for different boundary conditions to see the effects on the dynamics (Hossain & Mullan 1993). Computational domains are varied in order to see the effects of sound waves on the system. Calculations with different grid resolutions are performed to estimate the role of scale lengths on the problem. A detailed analysis of the simulations and their astronomical implications is given.

## 2. COMPUTATIONAL DETAILS

## 2.1. The PROMETHEUS code

The hydrodynamics code PROMETHEUS is based upon the piecewise-parabolic method (PPM, Colella & Woodward 1984). The method constructs the physics of the flow between grid points by a non-linear solution of the equations for conservation of mass, momentum, and energy (the Riemann problem) rather than the usual Taylor expansion about the grid points. This procedure affords greater resolution per grid point, which is highly desirable for multi-dimensional problems in stellar astrophysics. Although the computational effort required per grid point is higher than other commonly employed numerical methods, the number of grid points needed for a given level of accuracy is less (often much less). The net result for PPM is a *lower* total computational effort for given accuracies than competing numerical methods. Because the computational load per grid point is greater, a host of physics packages (nuclear reactions, radiation, gravity, etc.) may be added before affecting the runtime significantly. Thus PPM is well suited for multi-dimensional problems involving significant physics beyond the bare hydrodynamics.

The PROMETHEUS code was originally written by Bruce Fryxell and Ewald Müller, and is an extension of the basic PPM scheme in that (1) it includes an arbitrary number of separate fluids to account for abundances of nuclear species, (2) nuclear reactions and energy generation are taken into account, and (3) a realistic (not a gamma law) equation of state is used (Colella & Glaz 1985). Variations of this original code have been widely employed by other groups (e.g. Blondin & Lundqvist 1993, Burrows & Fryxell 1992), including one specifically for the study of convection in three dimensions (Cattaneo et al. 1991). PROMETHEUS can support different grid geometries, with cartesian, cylindrical, or spherical coordinates in 1, 2, or 3 dimensions as options. There is also an option of a moving grid, which allows a ‘semi-lagrangian’ approach to certain problems and adds greater resolution for problems where flows are significant across the entire grid, as in explosions.

## 2.2. Equation of State

The equation of state is the sum of components for electrons, ions, and radiation. The electron contribution is determined via cubic interpolation in tables for the thermal contributions (including  $e^+e^-$  pairs), plus degeneracy. Derivatives of the electron pressure and energy as functions of temperature and density are obtained from the direct differentiation of the interpolation functions. Table entries are logarithmically spaced both in temperature (in degrees Kelvin,  $\Delta\log(T) = 0.05$  from  $7 \leq \log(T) \leq 10$ ) and in density (in  $\text{gcm}^{-3}$ ,  $\Delta\log(\rho) = 0.125$  from  $2 \leq \log(\rho) \leq 10.5$ ). A perfect gas equation of state is smoothly joined for  $(\rho, T)$  regions not covered by the electron EOS table, and used for the ion EOS (to which a coulomb correction is added: Landau & Lifshitz 1969). Radiation pressure and energy density are included.

For the temperatures encountered in quiescent oxygen-burning, nuclear statistical equilibrium effects may be ignored, and the effects of quasi-equilibrium seem small. These effects are both ignored with regard to the equation of state.

### 2.3. Nuclear Reactions

The algorithms for nuclear reactions are similar to those used in prior quasi-static stellar evolution studies of massive stars (Arnett 1971). Twelve species ( $e^-$ , H, n,  $^4\text{He}$ ,  $^{12}\text{C}$ ,  $^{16}\text{O}$ ,  $^{20}\text{Ne}$ ,  $^{24}\text{Mg}$ , SiCa,  $^{56}\text{Ni}$ ,  $^{56}\text{Co}$ ,  $^{56}\text{Fe}$ ) are considered for the energy generation and nucleosynthesis resulting from pp, CNO, helium ( $3\alpha$ ), carbon, neon, oxygen, and silicon burning stages. The decays of  $^{56}\text{Ni}$  and  $^{56}\text{Co}$  are also included with density dependent decay rates (Fuller et al. 1985). The effects of *steady state* electron captures during oxygen and silicon burning are included; Urca processes and their attendant dynamic effects will be dealt with in subsequent work. The approximations in the reaction network used to represent oxygen and silicon burning are based upon extensive reaction network simulations (Thielemann & Arnett 1985, Arnett & Thielemann 1985, Arnett 1996).

Cooling by neutrino-antineutrino pair emission is included. This process has been identified in 1D stellar models (Arnett 1971) as competing with nuclear burning in a fashion that determines the thermal balance in the oxygen convective region. The thermal conditions of the flame zone, in particular, were determined by the bulk of the material in the convective region, which is  $\nu\bar{\nu}$  cooled, and advected into the flame zone. Using MLT, the heated material would then rise and cool by expansion and further  $\nu\bar{\nu}$  cooling. Thus, cooling by neutrino-antineutrino pair emission is never comparable locally to nuclear heating (Arnett 1969, Arnett 1971), rather it is the integral effect of heating and cooling across the convective zone which is important for thermal balance. We employ the pair emission rates of Beaudet et al. 1967, with small revisions for neutral current effects (Itoh et al. 1996).

### 2.4. Computational Differences

There are differences between these simulations and our exploratory work (Arnett 1994). Here we map the structure of the star resulting from one-dimensional hydrostatic calculations onto the upper and lower boundaries of the grid. Our previous work utilized constant entropy and isothermal outflow as the respective lower and upper boundary conditions. We calculate the 2D hydrodynamics from the outer region of the Si core to the H envelope, instead of just the O shell layer.

Another difference is the calculation of models with periodic boundary conditions. The initial work, as well as some of the simulations discussed here, were calculated with reflective boundary conditions, which are known to attract entrained flows and enhance the downward kinetic energy flux (Chan & Sofia 1986). Aside from not being realistic for sectors smaller than  $0 \leq \theta \leq \pi$ , reflective boundary conditions can also damp waves of wavelengths larger than the dimension of the calculation. Because we do not know exactly how power cascades to smaller scales in astrophysical conditions, as compared to box simulations with lower Reynolds' number, we find it to be prudent to use periodic boundary conditions rather than reflecting ones.

We have calculated models over a range of initial grid dimensions, grid resolutions, and boundary conditions to see how changes in any of these quantities would change the most critical results of this study. Table 1 shows the various descriptive qualities of the models. The differences are small (see Appendix). Most of the discussion is illustrated by the high resolution run, case D (460x128). A dominant constraint in choice of zoning is that the oxygen flame zone be well resolved (Arnett 1994).

#### 2.4.1. Numerical Effects

As a check of the robustness of our calculation, we have also run cases which have the same resolution, but a larger or smaller physical dimension. Calculations with a smaller physical domain are more sensitive to boundary conditions (and errors), so that larger domains are preferable. This is especially true for the oxygen shell burning epoch, because the other parts of the star are also evolving. The Si core is treated as an inert lower boundary; numerical experiments (to be reported separately) indicate that this approximation is valid over at least the early part of oxygen shell burning. The outer boundary is placed near the outer edge of the He core ( $M_r \approx 6M_\odot$ ). This insures that the acoustic flux is not artificially trapped, includes any back reaction from

Model	$n_r$	$n_\theta$	$\Delta r$	$\Delta\theta$	B. C. <sup>1</sup>
A	256	32	6.4e+10	$\frac{\pi}{2}$	P
B	256	64	6.4e+10	$\frac{\pi}{2}$	P
C	256	64	6.4e+10	$\frac{\pi}{2}$	R
D	460	128	6.4e+10	$\frac{\pi}{2}$	P
E	256	96	6.4e+10	$\frac{3\pi}{4}$	P

Table 1: Some Models in this Study.

---

<sup>1</sup>Boundary conditions: R and P denote reflective and periodic boundaries.

overlying burning shells, and allows us to construct a reasonable two dimensional approximation to a SN1987A progenitor model.

Cases A, B, and D of Table 1 provide a basis in which to examine effects of grid resolution; even the coarse case A gave qualitatively similar results. Case E tested the effect of a larger angular wedge (135 degrees instead of 90); the results were similar to case B.

The side boundaries provide a more serious challenge. Reflecting boundaries tend to trap waves, so that we have used periodic boundary conditions. Case C is identical to case B except for the use of reflecting instead of periodic boundaries; the effect is small for our simulations.

As an attempt to understand possible geometric peculiarities caused by the choice of grid geometry, we have used both an  $(r, \theta)$  coordinate system (Table 1), and some cases which used an  $(r, \phi)$  coordinate system (Bazán & Arnett 1994). The qualitative nature of the results is unaffected.

### 3. DISCUSSION

Convection in oxygen shells of massive stars is not driven in quite the same manner as convection in stellar envelopes or terrestrial phenomena. The equations to be solved look much like those of other compressible convection simulations,

$$\frac{\partial \rho}{\partial t} + \nabla \cdot (\rho \mathbf{v}) = 0, \quad (1)$$

$$\frac{\partial(\rho \mathbf{v})}{\partial t} + \nabla \cdot (\rho \mathbf{v} \mathbf{v}) = -\nabla p + \rho \mathbf{g}, \quad (2)$$

$$\begin{aligned} \frac{\partial(\rho E)}{\partial t} + \nabla \cdot (\rho \mathbf{v} E) &= -\nabla \cdot (p \mathbf{v}) - K(T, \rho) \nabla T \\ &\quad + \epsilon_{nuc}(X_i, \rho, T) - \epsilon_\nu(\rho, T) \end{aligned} \quad (3)$$

where  $E$  is given by,

$$E = \epsilon + \frac{1}{2} v^2, \quad (4)$$

and  $K(T, \rho)$  is the radiative conductivity. Notice, however, that there are source and sink terms for nuclear energy release and neutrino losses. Thus, we must solve a set of continuity equations for composition as well,

$$\frac{\partial(\rho X_i)}{\partial t} + \nabla \cdot (\rho X_i \mathbf{v}) = \rho \left( \frac{\partial X_i}{\partial t} \right)_{nuc}, \quad (5)$$

where, except for the factor of  $\rho$ , the right side is a system of reaction network equations. This means that convection in oxygen shells involves energy production and loss which is directly in the flow.



To our knowledge, the most physically similar system to have been examined previously with multi-dimensional simulations is the core helium flash (Cole & Deupree 1980, Deupree & Wallace 1987, Deupree 1996). The oxygen shell differs in that (1) the reaction rates involved have even more extreme temperature dependencies (roughly  $T^{40}$ ), (2) the equation of state is dominated by radiation and electron thermal pressures rather than degeneracy and thermal pressures, and (3) convection is driven by the competition between heating by nuclear burning and cooling by expansion and by neutrino emission (rather than cooling by radiative diffusion, as is the normal assumption in convective systems).

### 3.1. Timescales

The timescales of the problem portray this connection between convective mixing and energetics. Figure 1 shows the various timescales estimated from the MLT solution from the initial one-dimensional, hydrostatic stellar evolution model. The upper plot shows that the convective turnover time across a given radial grid zone,

$$t_{cnv} = \frac{\Delta x_i}{v_{cnv}}, \quad (6)$$

is very much shorter than either the nuclear energy timescale,

$$t_{nuc} = \frac{E_{th}}{|(\epsilon_{nuc}(X_i, \rho, T) - \epsilon_\nu(\rho, T))|}, \quad (7)$$

where  $E_{th}$  is the thermal component of the specific energy, or the Kelvin-Helmholtz timescale,

$$t_{KH} = \frac{\Omega}{L}, \quad (8)$$

where  $\Omega$  is the gravitational potential energy and  $L$  the luminosity (radiative and convective). This means that local convective response is fast enough to control heating and cooling. However, using MLT velocities, the integrated convective turnover time across the whole oxygen convective region is long ( $10^4$  seconds, or 550 sound travel times), so that the time to move material across the whole region is approaching both the nuclear timescale at the base of the convective shell ( $10^{4-5}$  seconds), and the neutrino Kelvin-Helmholtz timescale ( $10^{5-6}$  seconds) through the oxygen shell. This implies heterogeneity and significant nonspherical variation. The timescale for energy flow by radiative diffusion,

$$t_{rad} = \frac{\rho E_{th}}{|\nabla \cdot (K(T, \rho) \nabla T)|} \quad (9)$$

is orders of magnitude larger than all of these timescales, and, thus, is not important in this stage of evolution. For this reason, we need not calculate the effects of radiative diffusion in these simulations.

The lower plot shows the various abundance timescales, for nucleus  $i$ , where

$$t_i = X_i \left/ \left| \frac{\partial X_i}{\partial t} \right| \right. . \quad (10)$$

The burning timescale of oxygen is of the same order as the fastest convective timescale across a given grid zone, but orders of magnitude less than the turnover time across the convective region. Notice that many other nuclei have short timescales as well.

The magnitudes of these timescales lead us to several conclusions. First, *composition will not be homogeneous*. This will feed back into the structure via the energy source terms. Second, *the system has strong fluctuations in space and in time*. Because the thermal energy timescale is of the order of both the Kelvin-Helmholtz timescale and full convective mixing timescale, the

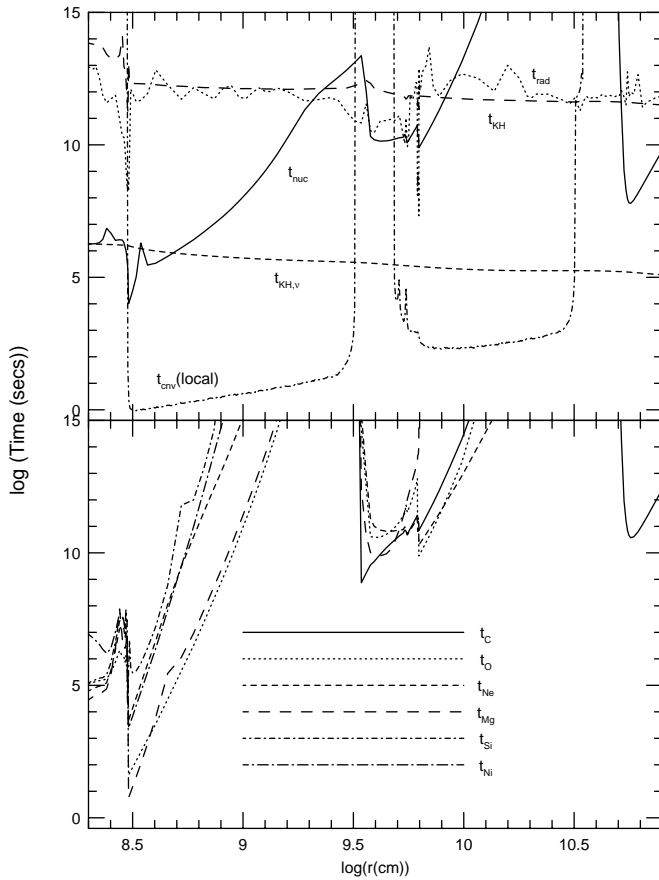


Fig. 1.— Timescales for Convection and Burning. Mixing and burn times are comparable.

dynamics of convection and evolution of the star will be strongly varying. This hardly satisfies the requirements of MLT which mandate that the dynamics of convection reach a statistical steady state. The energy supply changes as fast as convection can move energy across the region.

### 3.2. Evolution of the Velocity Field

Even at the beginning of our simulations, we see that MLT does not correctly represent the dynamics of convection in oxygen shells. Because the fluid transport timescales are initially longer than the oxygen burning time in the flame zone, the oxygen flame undergoes a initial thermal pulse, much like an AGB star (but faster), and a sound wave is emitted. This sound wave takes 18 seconds to cross the oxygen shell and effectively erases the MLT velocity field which we imposed initially. This allows the shell to establish dynamical structures from very low noise levels and reduces any worry that the initial perturbations somehow determine the final dynamical state. This pulse is not due to a faulty mapping of the initial model onto the 2D grid, but to an inconsistency between the assumed MLT physics of the convective shell, and the actual 2D hydrodynamics with heating and cooling. It is due to a thermal inconsistency involving assumed and actual convective cooling, not an error in overall hydrostatic balance.

Figure 2 shows snapshots of velocity evolution after times of 100, 200, 300, and 400 seconds. Before about 100 seconds, the dynamics are dominated by rising and descending plumes, which are driven by simple buoyancy. Small eddies (scale length  $\leq$  pressure scale height) form at the base of the shell and form/merge like those in most two dimensional convection simulations (Porter & Woodward 1994). By 200 seconds (11 sound travel times across the original oxygen convective zone), the region is fully convective and buoyancy braking is readily apparent as a retarding force to upward motions, causing swirls. A large eddy dominates the upper two-thirds of the convective region, and one eddy dominates in the lower third. At 300 seconds, a single downward plume spans the upper 2/3 of the zone, and buoyancy still dominates the flow dynamics. By 400 seconds, buoyancy braking affects the dynamics not only at the boundaries, but also throughout the zone.

These simulations exhibit many of the generic traits of multidimensional compressible turbulent convection simulations. A comparison of these vortices with other two-dimensional convection simulations (Hurlburt et al. 1986, Porter & Woodward 1994) shows that they are qualitatively similar in dimension (length/width  $\sim 1$ ), and that a few large eddies dominate. Porter & Woodward 1994 showed that this is to be expected, as two-dimensional simulations exhibit the merging of counterrotating eddies into larger ones. Earlier in our simulations, the lower 1/3 of the domain was populated by small eddies.

Velocity magnitudes in these eddies are typically at Mach numbers of 0.1 to 0.2, which is more than a factor of ten higher than MLT would predict. The spatial extent of these eddies is on the order of 3 pressure scale heights. The simulation at this epoch is still time dependent so that

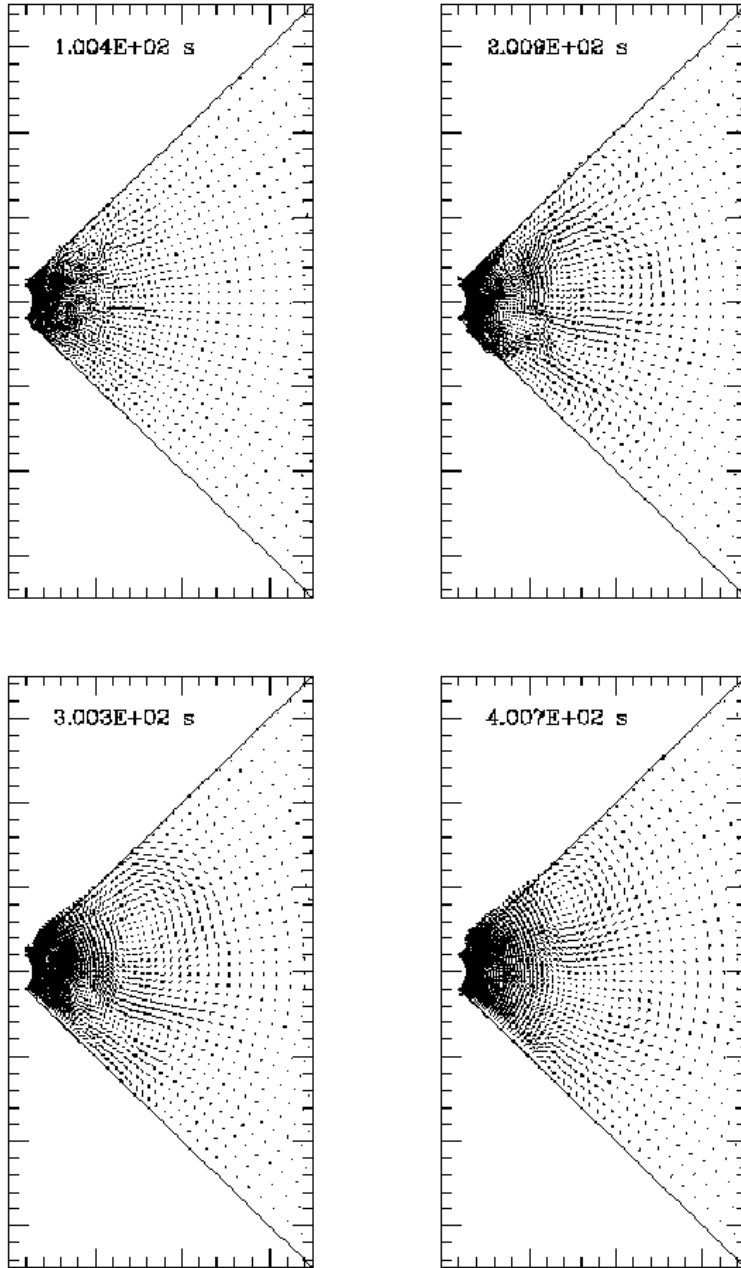


Fig. 2.— Snapshots of Velocity Fields, 100-400s. Large eddies dominate.

its structures should not be compared to the mixing length used in MLT. Only the radial velocity correlation length of a statistical steady state (Chan et al. 1982, Chan & Sofia 1989, Porter & Woodward 1994) should be used as some measure of a mixing length. As we explain later, the dynamical coupling of the energy generation to the kinematical mixing, as well as the limited number of convective turnover times involved in the entire stage of shell oxygen burning, prevents a statistical steady state from ever being attained in this stellar evolution stage.

In light of these results, *we view the details of one dimensional stellar evolution calculations of the structure of the oxygen shell with skepticism.* The smooth, steady flow assumed in those simulations appears to be a phenomenon which does not survive in more realistic calculations.

### 3.3. Energy Fluxes

The convective energy fluxes in this stage show both similarities and differences in comparison to previous compressible convection simulations. Figure 3 shows the azimuthally averaged enthalpy, kinetic, acoustic, and radiative fluxes after 400 seconds. The top panel shows the inner part of the O convective shell; the bottom panel gives the outer part, on different scales. Notice that the fluxes in the outer region are smaller in amplitude by more than a factor of 20. The enthalpy flux pictured here is *negative* through much of the Schwarzschild unstable region; MLT assumes it is positive. The formal convective boundaries are indicated as vertical dashed lines. The convective fluxes extend beyond these limits.

As in previous convection simulations, we find a non-zero flux of energy to be carried in the form of sound waves,

$$F_p = \overline{v_r \cdot \delta P}, \quad (11)$$

and kinetic energy,

$$F_k = \frac{1}{2} \left( \overline{\rho \mathbf{v} \cdot \mathbf{v} \mathbf{v}_r} \right). \quad (12)$$

MLT conventions require that the net radial kinetic energy flux be zero and that pressure equilibrium is always in effect. However, compressible convection simulations (Hurlburt et al. 1984, Chan et al. 1982, Chan & Sofia 1986, Cattaneo et al. 1991, Porter & Woodward 1994), reveal a finite kinetic energy flux due to cool, dense material being compressed into plumes. Since these plumes occupy a filling fraction at constant radius which conserves mass flux relative to slower, upward moving material, the kinetic energy flux must be nonzero. In this particular model, the kinetic energy flux can reach as much as 20 % of the enthalpy flux, which is less than the peak values of 60 % seen in previous “box” simulations. One explanation for this difference might be that simulations of convection in a box are governed by the competition between convective instability and viscous dissipation by radiative (or thermal) diffusion. Here, convective motion competes with neutrino losses, as well as numerical dissipation. The estimated radiative flux is

at least 4 orders of magnitude less than the enthalpy flux at all points in the simulation. This fact was emphasized in early stellar evolution studies of massive stars (Arnett 1972a), where MLT theory yielded the result that the luminosity at the boundary of such convective zones would be zero.

Figure 4 shows the enthalpy and kinetic fluxes and their sum at the top, middle, and bottom of the convective shell as a function of time. The dot-dashed curve is the kinetic flux, the dashed curve the convective flux, and the solid curve their sum. At no time during the simulation is the total luminosity equal to zero in the formally stable region. We note in passing that it is fortunate that neutrino losses govern the extent of this convection, since the numerical dissipation of the PPM method at this resolution (Porter & Woodward 1994), while yielding effective Reynolds’ numbers ranging from  $10^8$  at the base of the shell to  $10^5$  at the top, also imply Prandtl numbers ranging from 200 at the base to 1000 at the top. The small numerical dissipation is still larger than the tiny radiative dissipation. This suggests that we would need at least a tenfold increase in resolution before the radiative diffusion could be quantitatively evaluated, if at this tiny level it were still important.

An important component of the energy flow is the acoustic flux. This quantity measures the energy carried in the form of sound waves and is relevant to the kinetic energy flux in flows of significant Mach number (Hurlburt et al. 1984). In places the acoustic flux is a significant fraction of the kinetic flux. Thus, *any attempt to model systems such as these with implicit or anelastic*

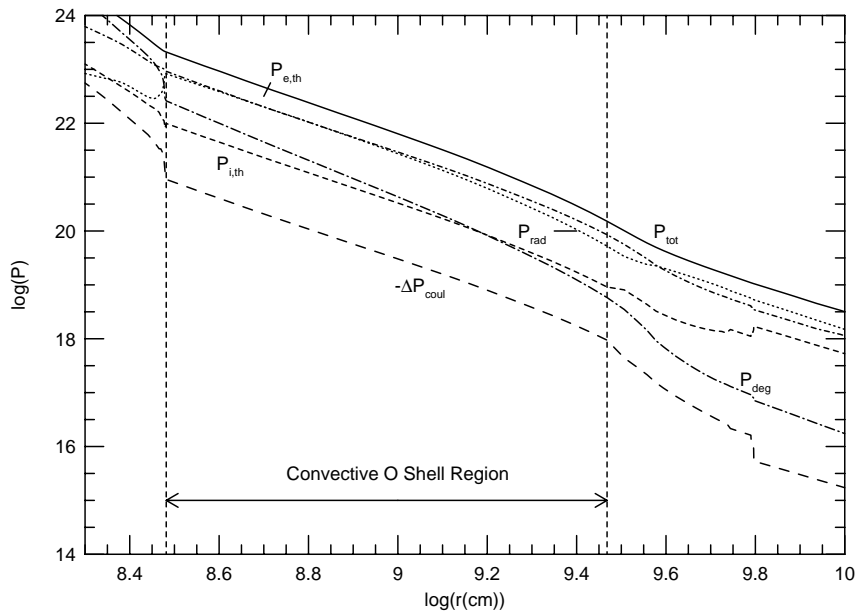


Fig. 3.— Pressure Contributions vs Radius. Thermal electron and radiation pressure dominate.

methods will miss the significant contribution to energy transport by sound waves.

The enthalpy flux distribution is negative through much of the Schwarzschild unstable domain. This is because the neutrino losses are dominant globally, causing contraction. After the first sound crossing time, the simulation adjusts to a state representative of the physics involved. The negative enthalpy flux implies that the energy arising from the oxygen burning flame zone is insufficient to support the structure predicted by MLT, and energy is being drawn from above. Neutrino-cooled matter is contracting down on the flame zone.

We find that there is a time dependance in many quantities throughout the duration of the simulation. For example, significant deviations in flux about an average value are seen in Figure 4.

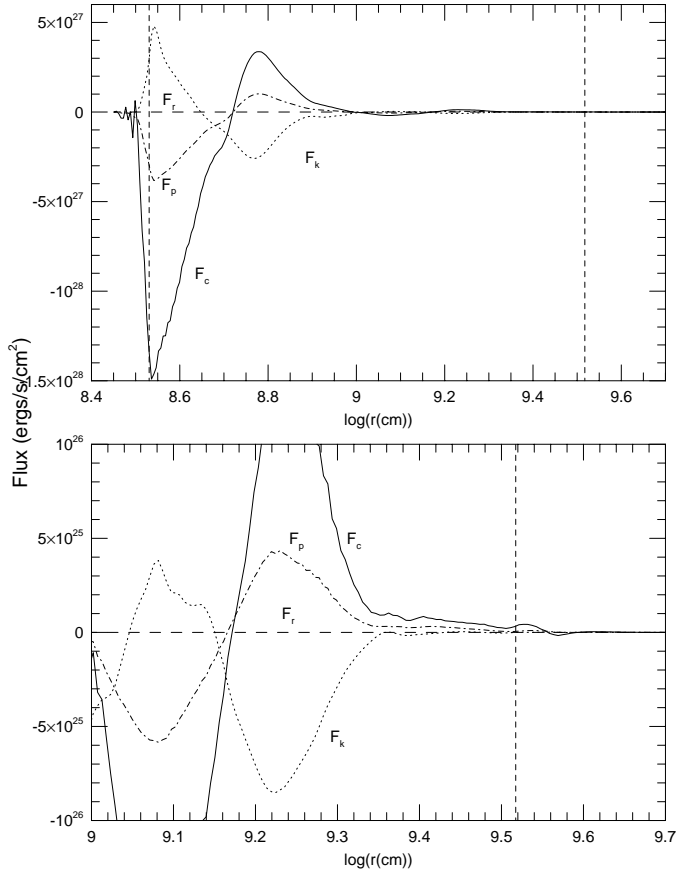


Fig. 4.— Energy Fluxes at 400s. Acoustic (p), kinetic energy (k), enthalpy (c), and radiative (r) fluxes are shown. Enthalpy flux is often *negative*, and acoustic and kinetic fluxes are important.

However, there may be a trend toward to a roughly constant amplitude for each of the three regions after 200s.

There are several reasons for the time variability in the simulation, and for it to continue until the time of core collapse. First of these are the similarities of both the nuclear and convective turnover timescales to the time left before core collapse. We estimate that there should be no more than 12 turnovers from the birth of the convective oxygen shell until core collapse, as estimated from our one-dimensional model. Previous box models of convection certainly required more turnovers before reaching a time-independent state (Hurlburt et al. 1984, Hurlburt et al. 1986). The other reason for time dependence in the simulation has to do with the density contrast and the aspect ratio. Previous work stressed that for density contrasts of 21, a minimum aspect ratio (horizontal /vertical dimensions) of about 3 was necessary for a static state to be reached in 80 turnover timescales (Hurlburt et al. 1984). In fact, since our simulation covers such a large spherical geometric area, the aspect ratio ranges from  $\sim 0.2$  at the base to  $\pi/2$  at the upper edge of the convective zone. Even for a  $2\pi$  simulation in  $r$  and  $\phi$ , rather than  $r$  and  $\theta$ , the ratio is only four times this value. Simulations still should be performed to see if these trends still hold in arbitrary geometries (cylindrical + spherical) as the effects of adiabatic cooling on individual mass elements is more enhanced in a curvilinear coordinate system than a cartesian system. Nevertheless, assuming the trends from the cartesian simulations roughly hold true in a spherical system, and that a density contrast of about 200 exists across the convective zone, and the values of our aspect ratios, our simulations suggest that *we can hardly expect this convective oxygen burning shell to ever reach a dynamical steady state before core collapse* and that *the application of mixing length theory in convective shell oxygen burning is unjustified*.

### 3.3.1. Penetration and Overshoot

We now consider the presence of overshoot in these calculations. The structure below and above the unstable region is not changed much from the initial state, hence the designation of *overshoot* and not *penetration*. As Figure 3 showed, thermal energy is transported out of the stable region while kinetic energy is transported into the region, apparently not in quantities sufficient to alter the structure in these regions. However, the structure of the temperature and density at the lower boundary is significantly altered. Most of this has to do with the mixing timescale being slower than the local oxygen burning timescale, in which case the oxygen is depleted and  $Y_e$  drops locally due to electron capture on the oxygen burning products. This, in turn causes changes in the entropy and composition, which then feeds back into the temperature and density.

*While these mass motions (Reynolds stresses) are not sufficient to alter the stellar structure significantly, they do allow mixing of composition from the convectively stable region into the unstable region.* Figure 5 shows the composition profiles of  $^{12}\text{C}$ . The  $^{12}\text{C}$  abundance in this



oxygen-burning convective shell is purely the result of undershoot from the upper,  $^{12}\text{C}$ -rich regions. A blob of  $^{12}\text{C}$  rich matter sinks down through the oxygen shell, finally halted by its own rapid burning. This is a new effect, not seen in one-dimensional simulations. We will discuss the consequences below.

Unlike the box simulations (Hurlburt et al. 1986, Hurlburt et al. 1994), we find that overshoot is more vigorous at the upper rather than the lower edge of the unstable region. This seems to be related to the relative stability of our upper and lower zones (Hurlburt et al. 1994). The presence of a nuclear shell at the bottom of the zone leads to a value of  $\gamma$  which changes faster as a function of position than it does at the top of the shell. This means that the *relative* stability

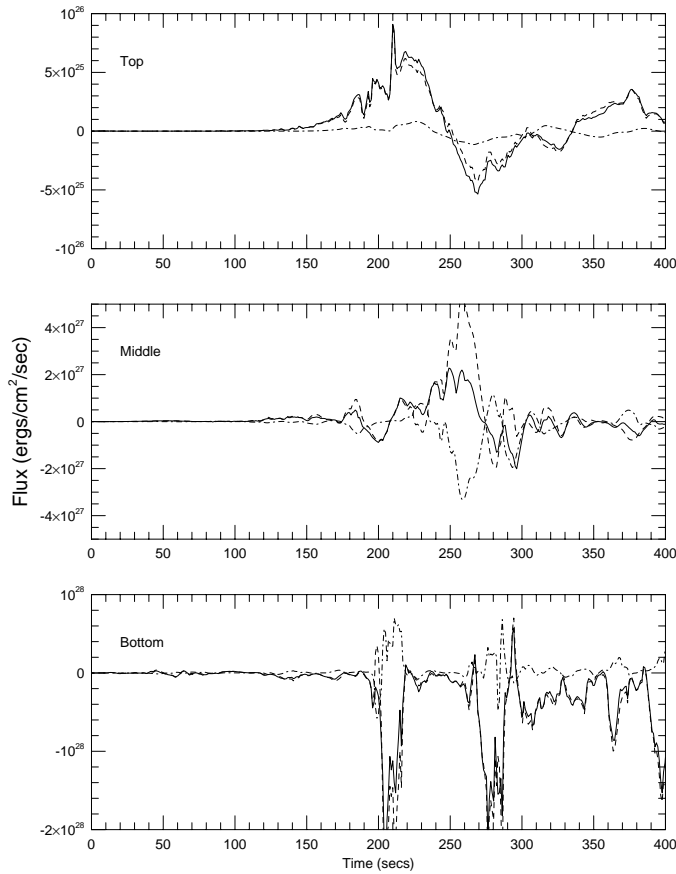


Fig. 5.— Energy Fluxes: time variability. Even with this low noise initial state, convection is well established after 200s, but highly variable.

of the bottom of the zone is higher than the top of the convective zone.

### 3.3.2. *Perturbations*

The early appearance of  $\gamma$ -lines from decay of  $^{56}\text{Ni}$ , as well as its effects on the light curve of SN 1987A, left theorists with the idea that mixing occurred, so that density and/or velocity perturbations must exist in the progenitor models (Chan & Lingenfelter 1987, Arnett 1988, Kumagai et al. 1988, Pinto & Woosley 1988). As hydrodynamical simulations have shown (Arnett et al. 1989, Fryxell et al. 1991, Müller et al. 1991, Herant & Benz 1992, Herant et al. 1992, Hachisu et al. 1992), these perturbations facilitate the mixing of  $^{56}\text{Ni}$  toward the surface through Rayleigh-Taylor instabilities. The exact details of the perturbations, such as scale distribution and amplitude, have not been self consistently examined, but linear analysis indicates that instabilities are likely at composition interfaces (Benz & Thielemann 1990, Müller et al. 1991).

Because of the behavior of the equation of state, as seen in its linearized form:

$$\begin{aligned} \frac{\delta P}{P} = & \frac{\delta \rho}{\rho} \left( \frac{P_{i,th} + P_{e,th} + \frac{4}{3}P_{deg}}{P} \right) \\ & + \frac{\delta T}{T} \left( \frac{P_{i,th} + P_{e,th} + 4P_{rad}}{P} \right) \\ & + \frac{\delta Y_e}{Y_e} \left( \frac{P_{e,th} + \frac{4}{3}P_{deg}}{P} \right) \\ & + \frac{P_{i,th}}{P} \left( \sum_j \frac{Y_j}{\sum_k Y_k} \frac{\delta Y_j}{Y_j} \right), \end{aligned} \quad (13)$$

the nonspherical perturbations are correlated, and show a strong temperature dependence due to the radiation pressure.

Figure 6 shows the different contributions to the pressure, as a function of radius. Electron degeneracy and thermal ion pressure contribute little to the total. Roughly 60 % is from thermal electrons, while almost all of the remaining 40 % is radiation pressure. This simplifies the above expression to one of the form:

$$\frac{\delta P}{P} = \frac{\delta \rho}{\rho} \left( \frac{P_{e,th}}{P} \right) + \frac{\delta T}{T} \left( \frac{P_{e,th} + 4P_{rad}}{P} \right) + \frac{\delta Y_e}{Y_e} \left( \frac{P_{e,th}}{P} \right). \quad (14)$$

This expression is a good description of the fluctuations in the flows.

In Figure 7, we show the density perturbation structure in and around the oxygen shell at the end of the calculation. The perturbation contours range over  $\pm 10\%$ . The largest perturbations are in the flame zone (the inner convective boundary), and at the outer convective boundary, as

may be seen in the right-hand panel. Notice that the thin flame zone, which lies near the leftmost arc in the left panel, has large perturbations in its small physical volume. The perturbations at the top of the convective zone have a much larger length scale, although their angular scales are similar to those in the flame zone. The “perturbation amplitudes” implied by the convection in the oxygen shell easily exceed the minimum needed to give significant mixing in supernova ejecta models (i.e. a few percent). Not surprisingly, the highest amplitude perturbations are found at the point where the linear analysis indicated: at the composition interfaces.

This may be sufficient to explain the mixing of most of the  $^{56}\text{Ni}$  observed in SN1987A, but apparently *not* that at highest velocity ( $v \approx 3,000 \text{ km s}^{-1}$ ; see Arnett 1991, Herant & Benz 1992). The production of this high velocity material may be related to the passage of the explosion shock,

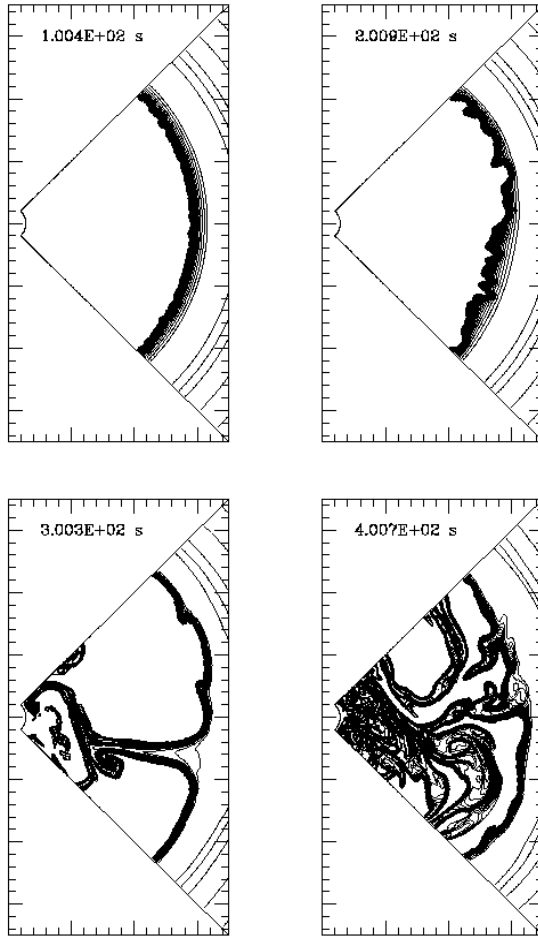


Fig. 6.—  $^{12}\text{C}$  Plume Snapshots. Such effects are not in 1D calculations.

and explosive oxygen burning in this inhomogeneous shell (Arnett 1994, Bazan and Arnett, in preparation). It might also be due to mixing outward by overshoot of  $^{56}\text{Ni}$  just prior to explosion (Herant & Benz 1992). This would require very high temperature oxygen burning; the silicon burning core has too large a neutron excess to produce  $^{56}\text{Ni}$ . We have seen no evidence for such high temperature oxygen burning; probably the best chance would be at the very onset of core collapse.

As with previous convection simulations (Hurlburt et al. 1986, Hurlburt et al. 1994), we conclude that gravity waves are responsible for the generation of the perturbations. A fourier analysis of the power in vertical velocities at different frequencies  $\nu$ , was made for the time interval

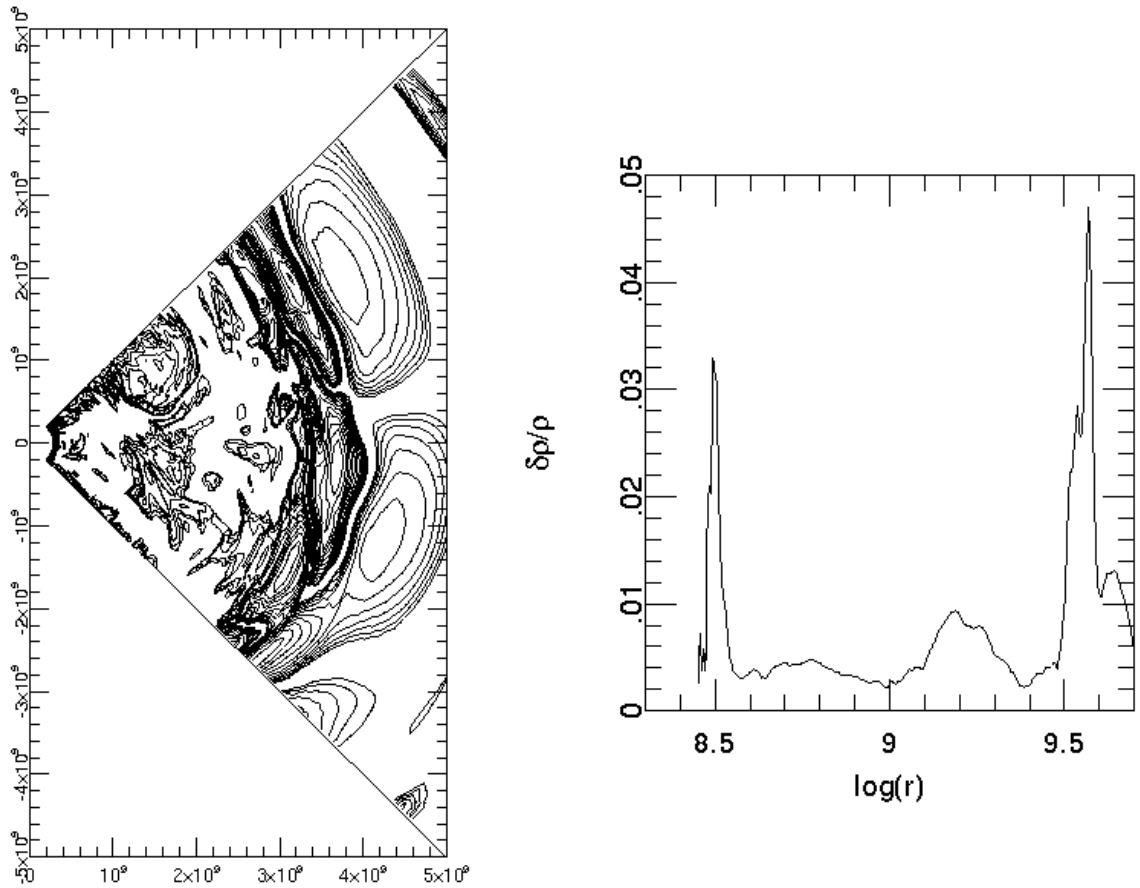


Fig. 7.— Density Perturbations at 400s. Left: Contours to  $\pm 10\%$ . Right: azimuthal averages (rms).

from 200 to 400s. Figure 8 shows the power as a function of frequency just above the convective zone (top panel), in the middle of the zone, and just below the convective zone (bottom panel); compare with Figure 4 of Hurlburt et al. 1986. The solid, dashed, and dot-dashed lines were taken at  $\frac{1}{4}, \frac{1}{2}, \frac{3}{4}$  of the angular domain. In the lower panel, we see the signature of a complex series of modes. The local Brunt-Vaisala frequency is  $N_{BV} = 1.55\text{s}^{-1}$ , which is much higher than most of the power. As did Hurlburt et al. 1986, we interpret this as a time variation due to internal gravity waves, recalling that such waves have frequencies less than the buoyancy frequency.

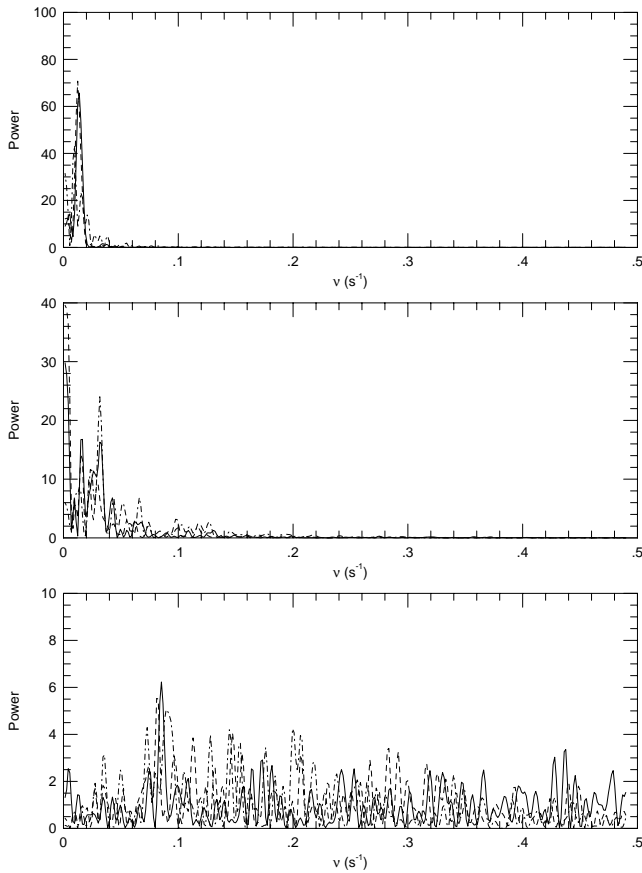


Fig. 8.— Power Spectrum over 200-400s, for top, middle and bottom of the convective region. At the top, most of the power is below the Brunt-Vässla frequency, indicating the importance of acoustic and gravity modes. The spread in power over frequencies at the bottom (flame zone) is due to extreme time variability.

However, just above the convective zone (top panel), we find that the power is also at frequencies just below the local Brunt-Vaisala frequency,  $N_{BV} \approx 0.02\text{s}^{-1}$ . The level of power here is larger, unlike Hurlburt et al. 1986, where the power above the convection zone was smaller than the power just below the convection zone. The difference seems to be in the nature of the driving and damping. In our simulation, the driving energy flux from the oxygen burning flame zone varies by factors of two at the base of the Schwarzschild unstable region. In addition, the energy release rate in the  $^{12}\text{C}$ -rich plume exceeds that from the oxygen flame. It has already been inferred that g-mode waves of high radial wave-number can appear at the interfaces between convectively stable and unstable regions (Press 1981, Hurlburt et al. 1986), and in this case we seem to have preferential driving of these modes.

While the appearance of g-mode wave interactions in this simulation is consistent other studies (Press 1981, Hurlburt et al. 1986), the details are different. Thermal diffusion is not present in this calculation, so that any damping of linear internal waves is the result of numerical dissipation (shocks). Pressure waves generated within the convective zone should have a constant horizontal wavenumber as their source. These internal waves are known to undergo internal reflection when  $N(r) = \omega$ , where  $N(r)$  is the Brunt-Väissala frequency at radius  $r$  (Press 1981). We note that the detailed coupling of acoustic and gravity waves to the convection also depends on boundary conditions (Hurlburt et al. 1994).

The greatest power in the middle of the convective zone occurs at zero frequency (center panel), as found by Hurlburt et al. 1986. However, despite our significantly better numerical resolution, our peaks are less well developed. We attribute this to the fact that our convection is much further from statistical relaxation. This is a physical feature of the epoch of oxygen shell burning, not a limitation of the simulation, as our previous discussion shows.

Figure 9 shows the power spectrum of density perturbations versus angular separations  $\Delta\theta$ , at 400s. Three radii are indicated: a solid line indicates a radius above the convective zone, a dot-dashed line the convective zone, and a dashed line a radius below the convective zone. There is a fall off at low angular separations,  $\Delta\theta \leq 0.1$ . The zoning is much finer than that, and will allow clumping on a much smaller scale ( $1/n_\theta \approx 0.008$ ). This fall off could be taken as a measure of the scale length of the perturbations to eventually be compared with observations, and as such is an important quantity, but two dimensional simulations such as these are biased. Because the vortices are pinned on the grid—their angular momentum vectors stay perpendicular to the plane of computation—cascading to smaller scales is inhibited. Thus we expect clumping down *at least* to scales this size; this issue must be addressed with fully three dimensional simulations.

### 3.4. Additional Convective Mixing

We mentioned that the asymmetry in the upflows and downflows has direct consequences for convective mixing. In Figure 6, we showed a time history of  $^{12}\text{C}$  abundance. In the initial model,  $^{12}\text{C}$  exists at the  $10^{-7}$  abundance level in the oxygen convective zone, and up to the 0.4 level above the zone. As rising material overshoots into the high  $^{12}\text{C}$  abundance area,  $^{12}\text{C}$ -rich matter is entrained. Eventually, cooling causes fast moving downward plumes to mix  $^{12}\text{C}$  deep into the convective zone. These fingers terminate at the point where  $^{12}\text{C}$  burns faster than it can be advected. Nuclear energy hot spots appear at these points, and by the end of the simulation the energy output from these hotspots are a factor of 30 higher than the oxygen flame zone itself. Even  $^4\text{He}$ , which exists still farther away from the MLT convection boundary, is brought down into the convective shell, albeit at a low level.

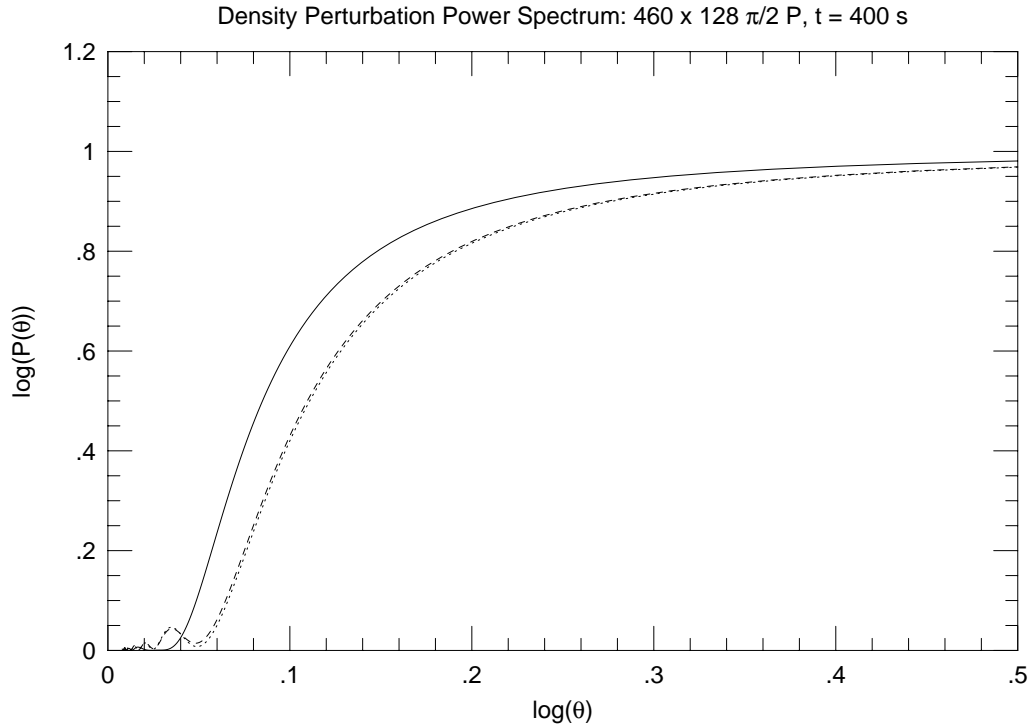


Fig. 9.— Power Spectrum of density perturbations versus angular separations  $\Delta\theta$ , at 400s.

An interesting phenomenon is the mixing of higher  $Y_e$  into the convective shell. Figure 10 shows the perturbation structure of the neutron excess  $\eta = 1 - 2Y_e$  at the end of the calculation. The non-uniform distribution at both the upper and lower boundaries is readily apparent. Since the ‘mass cut’ between the proto-neutron star and supernova ejecta is expected to occur within this convective zone, the presence of a non-uniform distribution of  $Y_e$  may alter core collapse (Burrows & Lattimer 1985, Burrows & Fryxell 1992). A larger effect could be from the coupling of the electron capture with hydrodynamics, which would change the entropy and the size of the core (Aufderheide 1993, Arnett 1996). Furthermore, once the delineation between neutron star and ejecta is made, explosive nucleosynthesis in the ejecta will reflect the distribution of neutron excess  $\eta$ . The differences of  $\Delta\eta \sim 0.002$  that we find here will radically alter the details of the

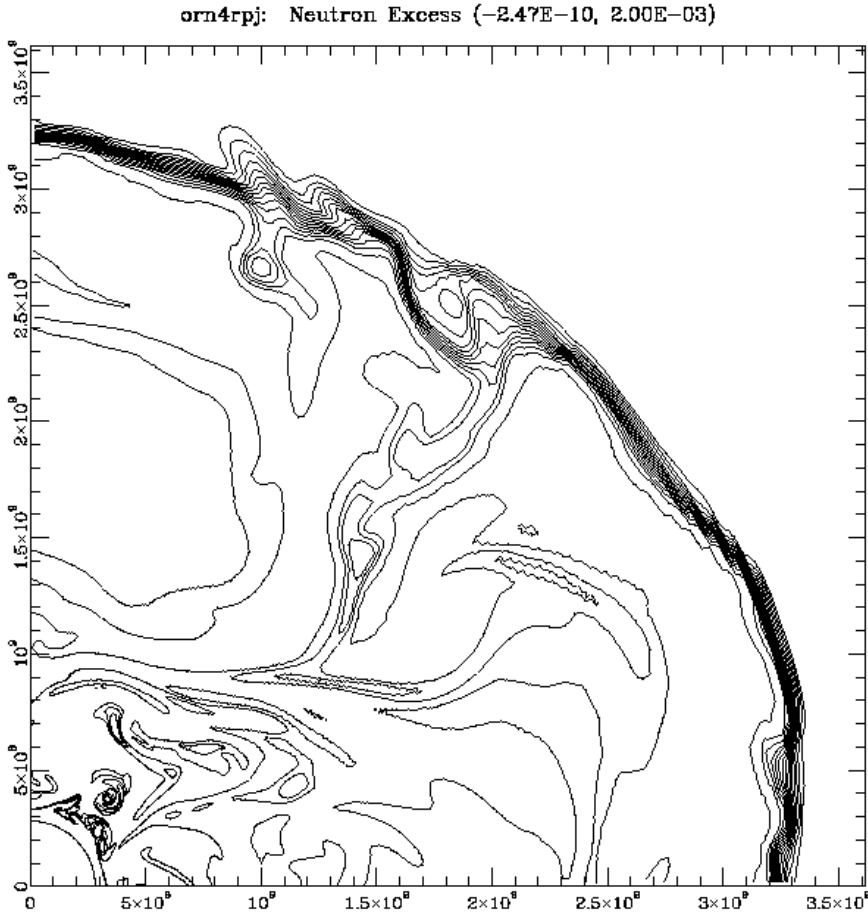


Fig. 10.— Contours of neutron excess  $\eta$ . Explosive nucleosynthesis yields are particularly sensitive to such variations. Twenty contours are plotted, linearly spaced from  $\eta = 0$  to  $\eta = 2 \times 10^{-3}$ .



quasi-statistical equilibrium (QSE) nuclear burning process (Truran et al. 1966, Michaud & Fowler 1972, Woosley et al. 1973) so that a non-uniform distribution of isotopes is produced. This may be a welcome result, as one dimensional models of explosive burning in massive stars have usually produced too many neutron-rich isotopes (Hainebach et al. 1974, Hartmann et al. 1985), unless the mass cut was carefully chosen (e.g., Thielemann, Hashimoto, & Nomoto 1990).

Most significantly, this extensive mixing by plumes may indicate that our concept of convection is too narrow to properly describe the neutrino cooled stages of massive star evolution. If this stage is so drastically altered, why not earlier stages as well?

### 3.5. Stellar Structure and Evolution

We have found that the results of our two-dimensional computations are inconsistent with 1D hydrostatic MLT results in many ways. As yet the evolution has proceeded about 10 % of the time from oxygen shell ignition to core collapse (for the 1D evolution of this initial model). What can we infer about 2D effects on evolution?

In 1D models, under MLT conventions, the O-burning region is wholly contained within the convective zone. This determines the evolution: the convective region burns until it changes its fuel to ashes, and there is little ingestion of new fuel or loss of ashes. Thus, at the exhaustion of fuel in the convective region, this layer of ashes is added to the underlying core. Contraction follows, and a new shell generally ignites just above the old, now defunct convective shell, and the process is repeated. This behavior has long been known (Rakavy, Shaviv, & Zinamon 1967, Arnett 1969); see Arnett 1996, §10.1 for details. Arnett 1972a noted its possibly non-physical nature, contrasted it to the case of a radiatively cooled shell, and also considered an alternative in which the convective region both lost ashes and ingested new fuel, so that it burned out in mass coordinate as a “wave.” However, we are aware of no published evolutionary sequences of neutrino cooled shells except those calculated with the implicit assumption that the first picture is correct. This distinction involves the nature of the *boundaries* of the convective region.

In these 2D simulations, within the first 25 seconds of evolution time, the flame zone ‘flashed’ and changed its thermodynamic state from convective instability to stability, thereby removing itself from the convective zone, as MLT would define it. The resulting sound wave does not develop into a shock as it moves down the density gradient. No structure changes occur by the passage of this wave.

The upper panel of Figure 11 shows the azimuthally averaged values of energy production, temperature, density, and convective speed, as a function of mass coordinate, for the initial and final state in this simulation (that is, at 0 and 400s). The variables of the initial model are represented by solid lines; those of the final model by dashed and by dotted lines. The most obvious difference is in the convective speed. In the initial (MLT) model, the velocities are

significant only in the convective oxygen burning shell and the convective helium burning shell. They are separated by a stable region containing C, Ne, Mg, and mostly O. In the final model, the convective speed is larger, and does not go to zero in this intermediate region. While in MLT the convective speed is a slowly varying quantity, in 2D simulations it fluctuates strongly.

This additional mixing has affected the composition structure, which is shown in the lower panel of Figure 11. This is especially noticeable in the range  $2.5 < M_r/M_\odot < 3.2$ . It is interesting that the He burning shell, which is broadened by radiative diffusion, widens more due to convection.

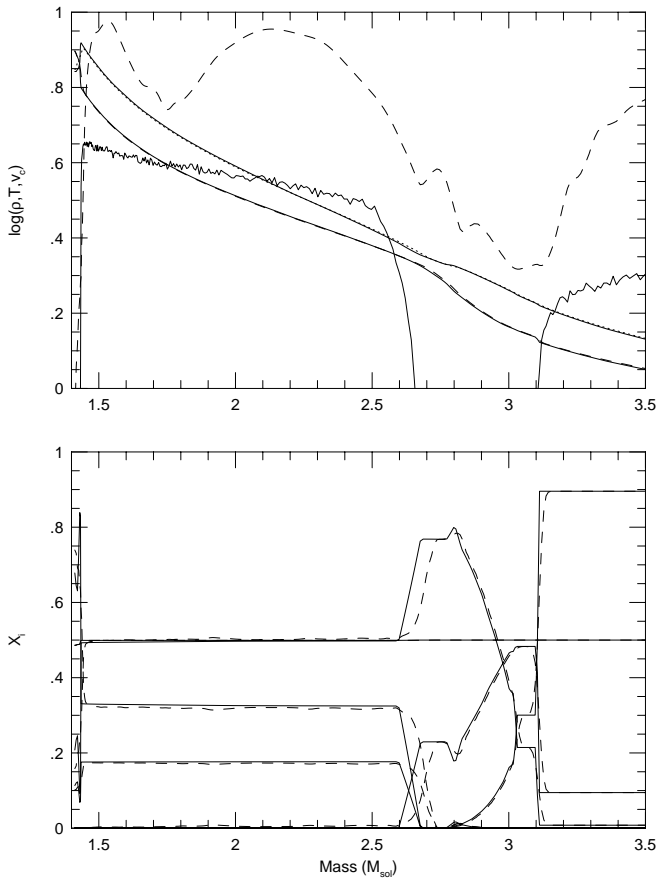


Fig. 11.— Top: Azimuthally averaged  $\epsilon$ ,  $\rho$ , and  $T$ , at 0 and 400s. Bottom: same for composition. While the gross structure is preserved, the flame zone changes. The velocity field is qualitatively different from 1D, allowing mixing across stable regions.

A second important difference is in the thin flame zone, which is strongly compressed in the mass coordinate, and therefore less obvious in Figure 11. Consider the temperature and density structure. Just above the inner boundary, the temperature has a small hole and the density a corresponding peak. At first sight, the run of both variables is almost identical between the initial and final models, but in fact the *boundary* has changed. The steep abundance gradient below the oxygen flame zone is becoming shallower, and the oxygen flame is no longer in the most convectively active region. Similarly, the outer edge of the temperature “hole” is smoothed out.

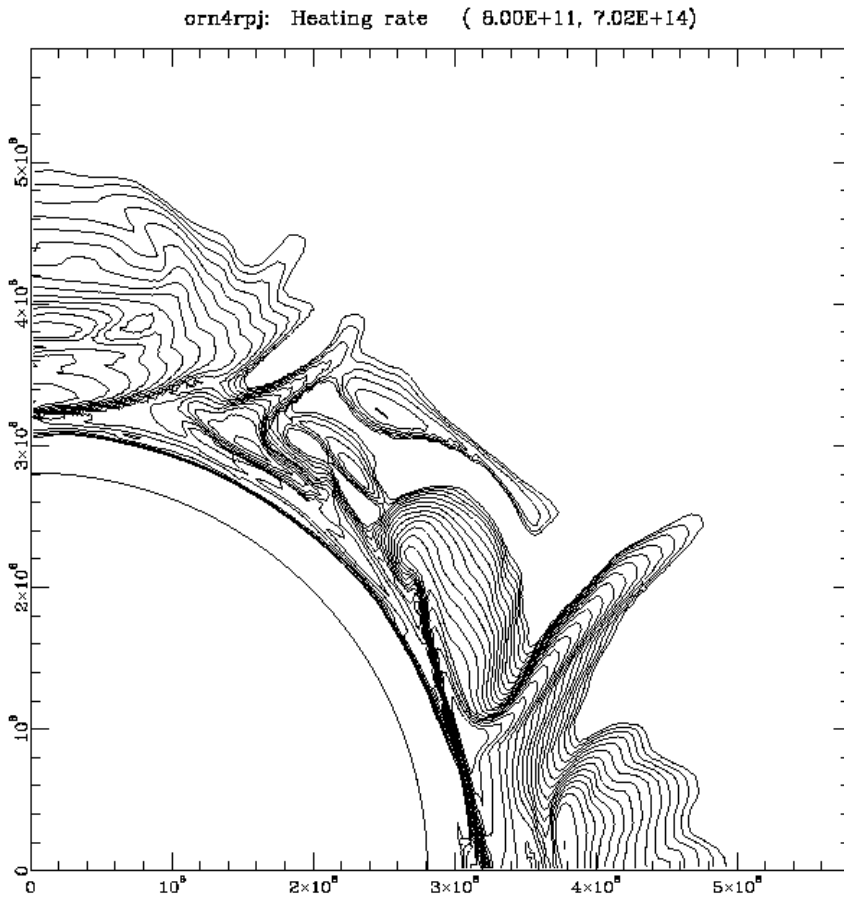


Fig. 12.— Closeup of Flame Region: Contours of the total rate of nuclear heating.

Figure 12 shows a closeup of the heating rate in the flame region. There is one velocity vector for each 25 zones. The 20 density contours are logarithmically spaced between  $\epsilon = 8.0 \times 10^{11}$  and  $7.0 \times 10^{14} \text{erg g}^{-1} \text{s}^{-1}$ . The oxygen burning shell is burning at  $\epsilon \leq 1.3 \times 10^{13} \text{erg g}^{-1} \text{s}^{-1}$ , and so is barely discernable as an inner ledge. The oxygen burning is not uniform, having several peaks.

Most of the energy release comes from carbon and neon burning, as blobs having  $X(^{12}\text{C})$  of a few percent burn vigorously. These conditions ( $T \approx 2.3 \times 10^9\text{K}$  and  $\rho \approx 8 \times 10^5\text{g/cc}$ ), occurring on a hydrodynamic time scale, are typical of “explosive nucleosynthesis” of carbon and neon.

Notice that the “hot spots” correspond to downward moving matter. The width of the whole flame zone is about 5 times wider than that of just  $X(^{16}\text{O})$ , and much more uneven. The velocities in the fastest burning zones (both oxygen and carbon) are relatively small, so the ashes are not immediately swept out into the most active convection.

This situation is drastically different from the conventional picture suggested by 1D models. It causes worry that the 2D evolution would have diverged from the 1D at a time even earlier than that for our initial model. We are currently attempting to push this sequence to later times (core collapse).

### 3.6. Dimensionality

Two dimensional simulations such as these clearly are more realistic than one dimensional simulations with ad hoc prescriptions for convection and mixing. Hydrodynamic flow is simulated self-consistently, and heterogeneity in space and time may be examined. Nevertheless, the assumed “rotational” symmetry (not presumed due to rotation but simply enforced by limitations in computational resources), is simply not valid. Simulation of a 3D sector, for example by extending the 460x128 by 64 zones in  $\phi$ , is feasible on a massively parallel supercomputer. We are currently continuing this calculation with a PVM version of PROMETHEUS, and will extend the simulations to three dimensions by the time of publication.

It is unclear at this time what physical state will be described by a three dimensional simulation. It is well known that the energy cascade in two dimensional turbulence (lower to higher scales) is opposite that in three dimensions (higher to lower scales). This effect can be seen quite easily in our and other PPM-based simulations (Porter & Woodward 1994), where small eddies disappear in favor of larger scale eddies. A recent comparison of two- and three-dimensional simulations of convection in a proto-neutron star (Müller & Janka 1997) also show an increase of small scale features in the three-dimensional simulation relative to the two-dimensional simulations, with an overall lower kinetic energy in the three-dimensional case. Thus, the overall convective and composition fields are expected to be more homogeneous in a three-dimensional case.

However, the effects of a third dimension on overshoot are not at all clear. This is critical for the oxygen shell evolution in light of what we mentioned previously concerning carbon brought into the oxygen shell by overshoot and the inhomogeneous energy release. On the one hand, we know that overshoot is the result of individual plumes creating gravity waves at convective stability/instability boundaries. Such plumes are known to be more energetic in three dimensions

than two due to a reduced drag effect (two dimensional ‘plumes’ are tori in reality) if starting from the same initial conditions. We know, though, that the initial underdensity which characterizes a plume is a function of the kinetic environment, which, from the supernova simulation mentioned above and turbulence studies, should be reduced from its two dimensional analog. Just which effect will predominate requires a three dimensional simulation. More insight can be obtained from laser experiments for related hydrodynamic problems, where Rayleigh-Taylor instabilities in 2D and 3D are examined experimentally within the context of inertial confinement fusion (Remington et al. 1995). Testing of PROMETHEUS against ICF codes and NOVA laser experiments is beginning (Kane et al. 1996).

#### 4. CONCLUSIONS

Direct calculation of the hydrodynamic behavior of oxygen burning shells indicates that the process is more interesting than previously supposed. Previous 2D work (Arnett 1994, Bazán & Arnett 1994) is confirmed and extended.

Composition is not homogeneous in the convective region. The system has strong fluctuations in both space and time. Mach numbers in the flow are typically 0.1 to 0.2; pressure fluctuations and acoustic fluxes are not negligible. Any attempt to model systems such as these with implicit or anelastic methods will miss the significant contribution of energy transport by sound waves. This convective flow will not reach a statistical steady state prior to core collapse. While the convective motions are not sufficient to alter the stellar structure significantly through their Reynolds stresses, they do allow mixing of composition from the convectively stable region into the unstable ones. The evolutionary implications of this have not yet been explored.

In light of these results, we view with skepticism the details of one dimensional stellar evolution calculations for this stage (e.g., Woosley & Weaver 1995, Thielemann, Hashimoto, & Nomoto 1990).

Prior to the core collapse, perturbations in density develop in the oxygen shell which are sufficiently large to “seed” hydrodynamic instabilities which will mix the “onion skin” composition of the presupernova. This occurs in precisely the region in which  $^{56}\text{Ni}$  is explosively produced by oxygen burning behind the explosion shock.

Although the active heating and cooling by nuclear burning and neutrino emission is novel, we find good agreement with previous multi-dimensional simulations of convection. Our results seem insensitive to numerical details.

Enlightening discussions with Prof. Phillip Pinto and Willy Benz are gratefully acknowledged. Information from Nick Brummell about work in progress is sincerely appreciated. This work was supported in part by NASA grant NAGW-2450, and by NSF grant ASTRO-9015976.

A. NUMERICAL EXPERIMENTS

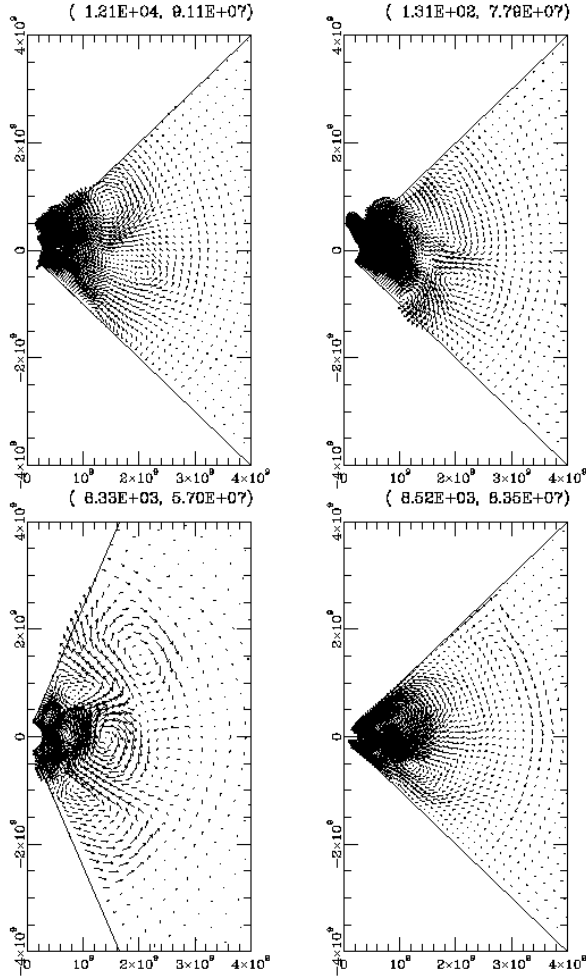


Fig. 13.— Velocity vectors for Models D (upper left), B (upper right), E (lower left), and C (lower right). See Table 1.

Figure 13 shows the velocity vectors for several numerical experiments: Models D, B, E, and C from Table 1. The two top panels show a change in resolution by a factor of 2 in each linear dimension. The higher resolution case is to the left. In the high resolution model, velocity vectors are the average vector over 4 zones, while the vectors in the lower resolution models of 90 and 120 degree extents are 2 and 3 zone averages, respectively. The flow patterns are qualitatively the same, and show some quantitative similarity as well, which leads us to believe that this resolution is the minimum needed for a ‘converged’ solution. The lower left panel shows the effect of widening the wedge from 90 to 120 degrees; we now have three vortices in the midlayer instead of two and

a half. A larger difference may be seen in the lower right panel, which used reflecting boundary conditions. The vortices are all contained within 90 degrees. Despite this, the qualitative features are still similar.

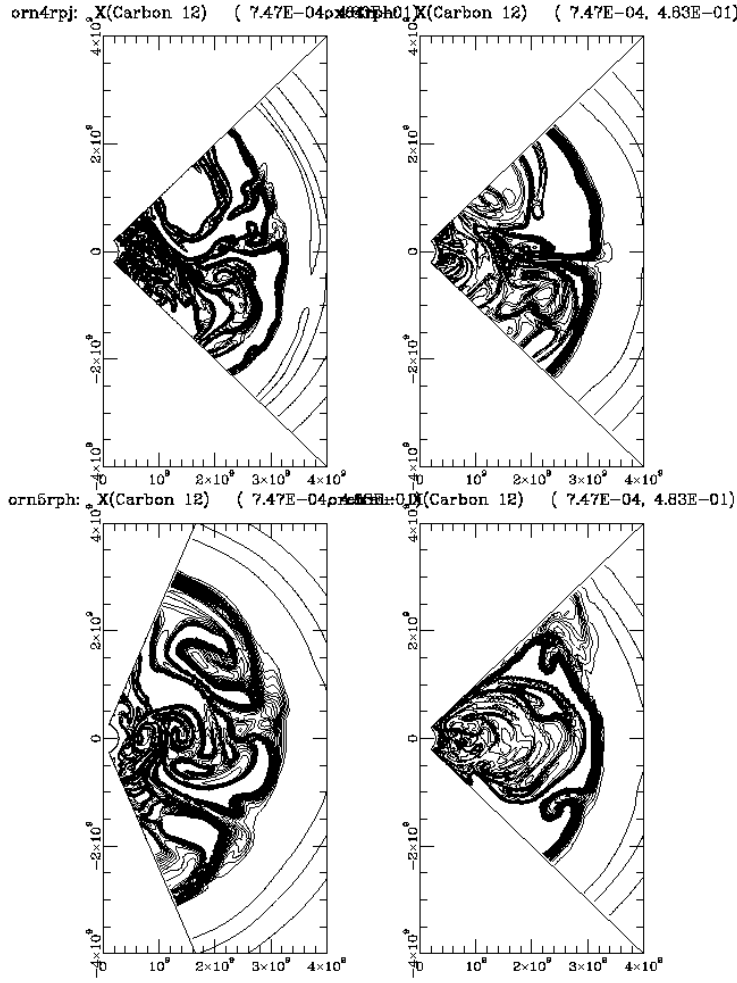


Fig. 14.— Abundance contours for  $^{12}\text{C}$  for models D, B, E, and C, as in Figure 13. See Table 1.

Figure 14 shows the corresponding panels for contours of  $^{12}\text{C}$  abundance. In all cases we have vigorous burning of an entrained plume of  $^{12}\text{C}$ -rich matter.

## REFERENCES

- Ait-Quamar, F., Kerrick, A. D., O'Neill, T. J., Tumer, O. T., Zych, A. D., & White, R. S. 1992, *ApJ*, 386, 715
- Arnett, W. D. 1969, in *Supernovae and Their Remnants*, ed. P. Branchio & A. G. W. Cameron, Gordon & Breach: New York
- Arnett, W. D. 1971, *ApJ*, 166, 153
- Arnett, W. D. 1972, *ApJ*, 173, 393
- Arnett, W. D. 1972, *ApJ*, 176, 699
- Arnett, W. D. 1977, *ApJ*, 218, 815
- Arnett, W. D. 1977, *ApJS*, 35, 145
- Arnett, W. D. 1988, in *Supernova 1987A in the Large Magellanic Cloud*, ed. M. Kafatos & A. G. Michalitsianos, Cambridge University Press: Cambridge, p. 301
- Arnett, W. D. 1991, *Ann. N. Y. Acad. Sci.*, 647, 1.
- Arnett, W. D. 1994, *ApJ*, 427, 932
- Arnett, W. D. 1996, in *Supernovae and Nucleosynthesis: A History of Matter from the Big Bang to the Present*, Princeton University Press: Princeton, NJ
- Arnett, W. D. & Thielemann, F.-K. 1985, *ApJ*, 295, 589
- Arnett, W. D., Fryxell, B. A., & Müller, E. 1989, *ApJ*, 341, L63
- Aufderheide, M. B. 1993, *ApJ*, 411, 813
- Bazán, G. & Arnett, W. D. 1994, *ApJ*, 433, L41
- Beaudet, G., Petrosian, V. & Salpeter, E. E. 1967, *ApJ*, 150, 979
- Benz, W. & Thielemann, F.-K. 1986, *ApJ*, 348, L17
- Blondin, J. & Lundqvist, P. 1993, *ApJ*, 405, 337
- Böhm-Vitense, E. 1958, *Z. Astrophys.*, 46, 108
- Bruenn, S. W. 1985, *ApJS*, 58, 771
- Burrows, A. & Lattimer, J. M. 1985, *ApJ*, 299, L19
- Burrows, A. & Fryxell, B. A. 1992, *Science*, 258, 430



- Canuto, V. M. & Mazzitelli, I. 1991, *ApJ*, 370, 295
- Canuto, V. M. 1992, *ApJ*, 392, 218
- Canuto, V. M. 1993, *ApJ*, 416, 331
- Cattaneo, F., Hurlburt, N. E., & Toomre, J. 1989, in *Stellar and Solar Granulation*, ed. R. J. Rutten & G. Severino, (Dordrecht: Kluwer), 415
- Cattaneo, F., Brummel, N. H., Toomre, J., Malagoli, A., & Hurlburt N. E. 1991, *ApJ*, 370, 282
- Chan, K. L., Sofia, S., & Wolff, C. L. 1982, *ApJ*, 263, 935
- Chan, K. L. & Sofia, S. 1986, *ApJ*, 307, 222
- Chan, K. L. & Sofia, S. 1989, *ApJ*, 336, 1022
- Chan, K. L. & Gigas, D. 1992, *ApJ*, 389, L87
- Chan, K. W. & Lingenfelter, R. E. 1987, *ApJ*, 218, L51
- Cole, P. W. & Deupree, R. G. 1980, *ApJ*, 239, 284
- Colella, P. & Glaz, H. M. 1985, *J. Comput. Phys.*, 59, 264
- Colella, P. & Woodward, P. R. 1984, *J. Comput. Phys.*, 54, 174
- Deupree, R. G. & Wallace, R. K. 1987, *ApJ*, 317, 724
- Deupree, R. G. 1996, *ApJ*, 471, 377
- Falk, S. W. & Arnett, W. D. 1973, *ApJ*, 180, L65
- Forestini, M., Arnould, M., & Lumer, E. 1991, *A&A*, 252, 127
- Fryxell, B. A., Müller, E. & Arnett, D. 1991, *ApJ*, 367, 619
- Fuller, G., Fowler, W. A. & Newman, G. 1985, *ApJ*, 293, 1
- Graham, E. 1975, *J. Fluid Mechanics*, 70, 689
- Graham, J. R. 1988, *ApJ*, 335, L53
- Hachisu, I., Matsuda, T., Nomoto, K., & Shigeyama, T. 1992, *ApJ*, 390, 230
- Hainebach, K. L., Clayton, D. D., Arnett, W. D., & Woosley, S. E. 1974, *ApJ*, 193, 157
- Hartmann, D., Woosley, S. E., & El-Eid, M. F. 1985, *ApJ*, 297, 837
- Herant, M. & Benz, W. 1992, *ApJ*, 387, 294

- Herant, M., Benz, W., & Colgate, S. 1992, ApJ, 395, 642
- Herant, M. & Woosley, S. E. 1994, 425, 814
- Hossain, M. & Mullan, D. J. 1991, ApJ, 380, 631
- Hossain, M. & Mullan, D. J. 1993, ApJ, 416, 733
- Hurlburt, N. E., Toomre, J., & Massaguer J. M. 1984, ApJ, 282, 557
- Hurlburt, N. E., Toomre, J., & Massaguer J. M. 1986, ApJ, 311, 563
- Hurlburt, N. E., Toomre, J., & Massaguer J. M., Zahn, J.-P. 1994, ApJ, 421, 245
- Itoh, N., et al., 1996, ApJS, in press (AAS CD-ROM Series, V, 1995)
- Kane, J., Arnett, D., Remington, B. A., Glendinning, S. G., Castor, J., Rubenchik, A., & Fryxell, B. A. 1997, ApJ, 478, L75
- Kumagai, S., Itoh, M., Shigeyama, T., Nomoto, K., & Nishimura, J. 1988, A&A, 197, L7
- Kumagai, S., Shigeyama, T., Nomoto, K., Itoh, M., Nishimura, J., & Tsuruta, S. 1989, ApJ, 345, 412
- Kurfess, J. D., Johnson, W. N., Kinzer, R. L., Kroeger, R. A., Strickman, M. S., Grove, J. E., Leising, M. D., Clayton, D. D., Grabelsky, D. A., Purcell, W. A., Ulmer, M. P., Cameron, R. A., & Jung, G. V. 1992, ApJ, 399, L137
- Latour, J., Toomre, J. & Zahn, J.-P. 1981, ApJ, 248, 1081
- Landau, L. D. & Lifshitz, E. M. 1959, *Fluid Mechanics*, (Addison-Wesley: Reading, MA).
- Landau, L. D. & Lifshitz, E. M. 1969, *Statistical Physics*, (Addison-Wesley: Reading, MA).
- Leising, M. D. & Share, G. H. 1990, ApJ, 357, 638
- Massaguer, J. M., Latour, J., Toomre, J., & Zahn, J.-P. 1984, A&A, 140, 1
- Michaud, G. & Fowler, W. A. 1972, ApJ, 173, 157
- Miller, D. S., Wilson, J. R., & Mayle, R. 1991, ApJ, 415, 278
- Müller, E., Fryxell, B. A., & Arnett, W. D. 1991, A&A, 251, 505
- Müller, E. & Janka, H.-T. 1997, A&A, 317, 140
- Palmer, D. M., Schindler, S. M., Cook, W. R., Grunsfeld, J. M., Heindl, W. A., Prince, T. A., & Stone, E. C. 1993, ApJ, 412, 203
- Pinto, P. A. & Woosley, S. E. 1988, ApJ, 329, 820

- Porter, D. H. & Woodward, P. R. 1994, *ApJS*, 93, 309
- Prandtl, L. 1925, *Z. Angew. Math. Mech.*, 5, 136
- Press, W. H. 1981, *ApJ*, 245, 286
- Rakavy, G., Shaviv, G., & Zinamon, A. 1967, *ApJ*, 150, 979
- Rast, M. P., Nordlund, A., Stein, R. F., & Toomre, J. 1993, *ApJ*, 408, L53
- Rast, M. P. & Toomre, J. 1993, *ApJ*, 419, 224
- Rast, M. P. & Toomre, J. 1993, *ApJ*, 419, 240
- Remington, B. A. et al., 1995, *Phys. Plasmas*, 2, 241
- Renzini, A. 1987, *A&A*, 188, 49
- Schmitt, J. H. M. M., Rosner, R., & Bohn, H. U. 1984, *ApJ*, 282, 316
- Sofia, S. & Chan, K. L. 1984, *ApJ*, 282, 550
- Spiegel, E. A. 1963, *ApJ*, 138, 216
- Stein, R. & Nordlund, A. 1989, *ApJ*, 342, L95
- Thielemann, F.-K. & Arnett, W. D. 1985, *ApJ*, 304, 619
- Thielemann, F.-K., Hashimoto, M., & Nomoto, K. 1990, *ApJ*, 349, 222
- Toomre, J., Brummell, N. H., Cattaneo, F., & Hurlbert, N. E. 1990, *Comp. Phys. Comm.*, 59, 105.
- Truran, J. W, Cameron, A. G. W., & Gilbert, A. 1966, *Can. J. Phys.*, 44, 563
- Tueller, J., Barthelmy, S., Gehrels, N., Teegarden, B. J., Leventhal, M., & MacCallum, C. J. 1990, *ApJ*, 351, L41
- Vitense, E. 1953, *Z. Astrophys.*, 32, 135
- Woodward, P. R., & Colella, P. 1984, *J. Comput. Phys.*, 54, 115
- Woosley, S. E., Arnett, W. D., & Clayton, D. D. 1972, *ApJ*, 175, 731
- Woosley, S. E., Arnett, W. D., & Clayton, D. D. 1973, *ApJS*, 26, 231
- Woosley, S. E., & Weaver, T. A. 1995, *ApJS*, 101, 181
- Xiong, D. R. 1985, *A&A*, 150, 133
- Zahn, J.-P. 1991, *A&A*, 252, 179